Modeling Earth Systems and Environment (2019) 5:1853–1865
https://doi.org/10.1007/s40808-019-00643-6

ORIGINAL ARTICLE

A reaction–diffusion mathematical model on mild atherosclerosis

Debasmita Mukherjee[1] · **Lakshmi Narayan Guin**[1] · **Santabrata Chakravarty**[1]

Received: 21 July 2019 / Accepted: 3 September 2019 / Published online: 16 September 2019

Abstract
The evolution of atherosclerotic plaque is in general a complex phenomenon, which is yet to be perceived completely. The present work deals with a simple reaction–diffusion model system to describe the early onset of atherosclerotic plaque formation. Both the non-spatial and spatial systems are studied analytically and numerically. The non-spatial system has been found to be globally stable, and hence, it can withstand considerable variation in parameter values leading to some assistance for various clinical investigations on atherosclerosis. The results based on model parameter values reveal several bifurcation diagrams with respect to significant model parameters with biological implications for the non-spatial system. Moreover, necessary condition for diffusive instability of a locally stable equilibrium is included in the present work to understand the dynamical behaviour of the system.

Keywords Atherosclerosis · Reaction–diffusion system · Global stability · Saddle-node bifurcation

Mathematics Subject Classification 34D23 · 37G35 · 34C23 · 34K18

Introduction

Atherosclerosis is a chronic inflammatory disease occurring due to plaque accumulation in the innermost layer of the artery. It is the primary cause of heart attack (acute myocardial infarction) and stroke (cerebrovascular accident), resulting in 900, 000 deaths per annum in US in particular and 13 million death worldwide, in general (Hao and Friedman 2014).

Atherosclerosis is a non-symptomatic disease, which takes about 14–15 years to produce symptoms and can start as early as from infancy. Numbness or pain in certain body parts is the early symptoms of this disease depending on the site where the plaque builds up (Ougrinovskaia et al. 2010). Usually, atherosclerotic plaque consists of low-density lipoprotein (LDL), macrophages, smooth muscle cells (SMCs), platelets, and debris. The plaque builds up in the intima, and in the long run, it grows beyond a certain limit exerting immense pressure on the endothelium wall. Then, endothelium wall breaks down and the plaque bulges into the lumen which restrains smooth blood flow in those body parts causing pain or numbness as the early symptoms of atherosclerosis (Libby et al. 2002).

A large number of clinical investigations (Libby et al. 2002; Malek et al. 1999; Gijsen et al. 2008) confirm that the process of atherosclerotic plaque formation starts with a lesion in the endothelium wall. Smoking is one of the leading causes of endothelial lesions (Pittilo 2000). Bad cholesterol, that is, LDL enters into the intima through those endothelial lesions and gets oxidised in the presence of free radicals in the intima. The immune response to this oxidation process signals endothelium cells to recruit monocytes and T cells. In intima, monocytes are differentiated into macrophages in the presence of scavenger receptors. Macrophages phagocytose oxidised LDL particles and eventually form foam cells (lipid-laden cells) (Little et al. 2009; Johnson and Newby 2009; Gui et al. 2012). Foam cells together with the dead macrophages, cell debris form atherosclerotic plaque.

Since the atherosclerotic plaque formation usually takes about 14–15 years to become symptomatic, its clinical

✉ Santabrata Chakravarty
santabrata.chakravarty@visva-bharati.ac.in

Debasmita Mukherjee
debasmita.sarada@gmail.com

Lakshmi Narayan Guin
guin_ln@yahoo.com

[1] Department of Mathematics, Visva-Bharati, Santiniketan 731235, WB, India

investigations are very expensive and time consuming. Various mathematical models were made use of to study the mechanism of interactions of the cellular components over the past few years (Hao and Friedman 2014; Ougrinovskaia et al. 2010; McKay et al. 2005; Cobbold et al. 2002; Cohen et al. 2014; Bulelzai and Dubbeldam 2012; Anlamlert et al. 2017; Ibragimov et al. 2005; Friedman and Hao 2015), to investigate the dynamical response of atherosclerotic plaque models. An extensive list of previous work done on atherosclerosis can be found in Parton et al. (2015). Very recently, a mathematical model was proposed by Guo et al. (2018) with the introduction of intraplaque neovascularisation and hemodynamic computation with plaque destabilisation for the purpose of having an estimate of the effect of neo-angiogenesis and intraplaque haemorrhage in the formation of atherosclerotic plaque quantitatively. With the advancement of matured plaques, vascular smooth muscle cells are replenished from media to synthesise a fibrous cap that stabilises the plaque and sets apart the plaque content from bloodstream. The fibrous cap protects against the clinical issue of atherosclerosis. For reasons unknown, it is often observed that certain plaques become stable and robust, while others become fragile and alarmingly sensitive to rupture. With this motivation, a multiphase model has been taken up by Watson et al. (2018) subsequently to investigate early fibrous cap formation in the atherosclerotic plaque. The present authors' recent work (Mukherjee et al. 2019) comprises of a nonlinear ODE model of atherosclerosis including ten relevant cellular components involved in the plaque formation process. The model is subsequently reduced with quasi-steady-state approximation theory. A detailed analysis of the reduced model has been performed there and effect of the wall shear stress of the artery wall in atherosclerosis is adequately incorporated.

The present article focuses on a simplified model comprising the basic interaction of macrophage phagocytosing oxidised LDL in atherosclerotic plaque formation. A reaction–diffusion model system of two partial differential equations involving one-spatial dimension is being considered to address the phagocytosing process. The present model can be biologically interpreted as, even a small perturbation in the non-inflammatory state can lead the chronic inflammatory reaction in presence of large LDL concentrations.

In "Formulation of the model", an one-dimensional reaction–diffusion model of atherosclerosis is introduced; in "Rescaled model", the model is duly non-dimensionalised, while the stability analysis of the non-spatial model is provided in "Kinetic model". "Stability analysis in the presence of diffusion" deals with the stability analysis of the spatial model system; "Numerical simulation" takes into account the numerical simulation and discussion of the results obtained, and finally, "Concluding remarks" covers the concluding part of this article.

Formulation of the model

To represent the biochemical process through a suitable mathematical model, a few assumptions are being considered. The present model is focused on the key aspects of the plaque formation process. Only the interactions between oxidised LDL and macrophages are considered for the model formulation.

The basic equations over a domain $\Omega = [0, L] \subseteq \mathbb{R}$ as described in Fig. 1 inside the intima, under the assumption that oxidised LDL (X) and macrophages (M) are diffusing according to Fick's law in Ω are:

$$\frac{\partial \tilde{X}}{\partial \tilde{t}} = K - \rho_1 \frac{\tilde{M}\tilde{X}}{\delta + \tilde{X}} - d_X \tilde{X} + \gamma_1 \tilde{\nabla}^2 \tilde{X}, \tag{2.1}$$

$$\frac{\partial \tilde{M}}{\partial \tilde{t}} = D\tilde{X} + fR(\tilde{X}, \tilde{M})\tilde{X}\tilde{M} - \rho_2 \frac{\tilde{M}\tilde{X}}{\delta + \tilde{X}} - d_M \tilde{M} + \gamma_2 \tilde{\nabla}^2 \tilde{M}, \tag{2.2}$$

where $\tilde{\nabla}^2 \equiv \frac{\partial^2}{\partial \tilde{x}^2}$, with the initial conditions $\tilde{X}(0, x) \geq 0$, $\tilde{M}(0, x) \geq 0, \forall x \in \Omega$. The domain being considered is entirely within intima, and so, boundary conditions can be assumed to be zero-flux conditions $\frac{\partial \tilde{X}}{\partial n} = \frac{\partial \tilde{M}}{\partial n} = 0$ in $\partial\Omega \times (0, \infty)$, where n is the outward normal vector of the boundary $\partial\Omega$, which is assumed to be smooth. The choice of such boundary conditions implies that the oxidised LDL and the macrophages cannot leave the domain during the plaque formation process.

Equation (2.1) denotes the evolution of concentration of oxidised LDL as long term oxidised LDL influx rate K (Ougrinovskaia et al. 2010), ingestion of oxidised LDL by macrophages $\rho_1 \frac{\tilde{M}\tilde{X}}{\delta + \tilde{X}}$, loss of oxidised LDL $d_X \tilde{X}$, and the corresponding diffusion term $D_1 \tilde{\nabla}^2 \tilde{X}$. Equation (2.2) represents the change of concentration of macrophages as macrophage influx $D\tilde{X} + fR(\tilde{X}, \tilde{M})\tilde{X}\tilde{M}$ (Ougrinovskaia et al. 2010), reduction in macrophage capacity due to phagocytosing oxidised LDL $\rho_2 \frac{\tilde{M}\tilde{X}}{\delta + \tilde{X}}$, death of macrophages $d_M \tilde{M}$, and the corre-

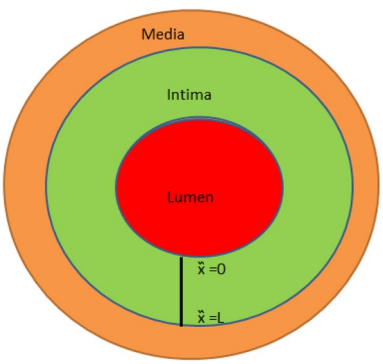

Fig. 1 Cross-section of an artery

sponding diffusion term $D_2\tilde{\nabla}^2\tilde{M}$. The parameters K, D, f have similar meaning as of Ougrinovskaia et al. (2010) and δ is the half-saturation constant.

Rescaled model

For rescaling purpose, as in Ougrinovskaia et al. (2010), $R(\tilde{X},\tilde{M}) = 1$ is assumed:

$$\frac{\partial X}{\partial t} = d_{11} - d_{12}\frac{MX}{1+X} - X + D_1\nabla^2 X, \tag{3.1}$$

$$\frac{\partial M}{\partial t} = d_{21}X + d_{22}XM - d_{23}\frac{XM}{1+X} - d_{24}M + D_2\nabla^2 M, \tag{3.2}$$

where,

$$X = \tilde{X}/\delta,\ M = \tilde{M}/\delta,\ t = \tilde{t}d_X,\ x = \frac{\tilde{x}}{L},$$
$$d_{11} = \frac{K}{\delta d_X},\ d_{12} = \frac{\rho_1}{d_X},$$
$$D_1 = \frac{\gamma_1}{d_X L^2},\ d_{21} = \frac{D}{d_X},\ d_{22} = \frac{\delta f}{d_X},\ d_{23} = \frac{\rho_2}{d_X},$$
$$d_{24} = \frac{d_M}{d_X},\ D_2 = \frac{\gamma_2}{d_X L^2}.$$

Kinetic model

To determine various conditions for the onset of inflammatory reaction, first, one should consider only the reaction part of the system (3.1)–(3.2), as follows:

$$\frac{\mathrm{d}X}{\mathrm{d}t} = d_{11} - d_{12}\frac{MX}{1+X} - X, \tag{4.1}$$

$$\frac{\mathrm{d}M}{\mathrm{d}t} = d_{21}X + d_{22}XM - d_{23}\frac{XM}{1+X} - d_{24}M, \tag{4.2}$$

with initial conditions $X(0) \geq 0,\ M(0) \geq 0$.

Stability analysis of the kinetic model

Positivity and boundedness

Theorem *Let all the parameters of the system of Eqs. (4.1)–(4.2) be positive and Γ be a region in $\mathbb{R}^2_+$ defined as, $\Gamma = \{(X,M) \in \mathbb{R}^2_+ | 0 \leq X \leq \bar{X}, 0 \leq M \leq \bar{M}\}$. Then, Γ is positive invariant and all the solutions starting from Γ are uniformly bounded, and the parameters over bar are being the respective upper bounds.*

Proof First, one may make an attempt to prove the positive invariant part.

Let $(X(0), M(0)) \in \Gamma$.

If possible, suppose $X(t)$ be non-positive. Then, there exists $t_0 > 0$, such that $X(t_0) = 0$ and $X(t) > 0$ for any t satisfying $0 \leq t \leq t_0$. Then, necessarily

$$\frac{\mathrm{d}X}{\mathrm{d}t}|_{t=t_0} \leq 0.$$

This is a contradiction, because

$$\frac{\mathrm{d}X}{\mathrm{d}t}|_{t=t_0} = d_{11} - d_{12}\frac{M(t_0)X(t_0)}{1+X(t_0)} - X(t_0) = d_{11} > 0.$$

Hence, $X(t)$ is positive $\forall t \geq 0$. Similarly,

$$\frac{\mathrm{d}M}{\mathrm{d}t}|_{t=t_0} = d_{21}X(t_0) + d_{22}X(t_0)M(t_0) - d_{23}\frac{X(t_0)M(t_0)}{1+X(t_0)} - d_{24}M(t_0) = d_{21}X(t_0) > 0.$$

Hence, $X(t)$ is positive $\forall t \geq 0$. Next, the part of boundedness may be shown as follows:

From Eq. (4.1), one may have:

$$\frac{\mathrm{d}X}{\mathrm{d}t} = d_{11} - d_{12}\frac{MX}{1+X} - X$$
$$\implies \frac{\mathrm{d}X}{\mathrm{d}t} + X \leq d_{11}$$
$$\implies X(t) \leq d_{11} + \kappa_1 e^{(-t)},$$

where κ_1 is a positive integrating constant. The term $\kappa_1 e^{-t}$ vanishes as $t \to \infty$. Therefore, $X(t) \leq d_{11}$ as, $t \to \infty$, i.e., $X(t)$ remains bounded $\forall t \geq 0$. Then, one may choose α_2, a positive constant, such that $d_{22}X \leq \alpha_2 \leq d_{24}$. Next

$$\frac{\mathrm{d}M}{\mathrm{d}t} = d_{21}X + d_{22}XM - d_{23}\frac{XM}{1+X} - d_{24}M$$
$$\implies \frac{\mathrm{d}M}{\mathrm{d}t} + d_{24}M \leq d_{21}X + d_{22}XM$$
$$\leq \alpha_1 + \alpha_2 M$$
[as X is bounded so one may assume $d_{21}X \leq \alpha_1$, a positive constant]
$$\implies \frac{\mathrm{d}M}{\mathrm{d}t} + (d_{24} - \alpha_2)M \leq \alpha_1$$
$$\implies M(t) \leq \frac{\alpha_1}{d_{24} - \alpha_2} + \kappa_2 e^{(-(d_{24}-\alpha_2)t)},$$

where κ_2 is a positive integrating constant. The term $\kappa_2 e^{(-(d_{24}-\alpha_2))t}$ vanishes as $t \to \infty$, because $(d_{24} - \alpha_2) \geq 0$. Therefore, $M(t) \leq \frac{\alpha_1}{d_{24}-\alpha_2}$ as, $t \to \infty$, i.e., $M(t)$ remains bounded $\forall t \geq 0$ (Anlamlert et al. 2017).

Equilibrium points and their stability

The system (4.1)–(4.2) has a non-zero equilibrium position $E(X_e, M_e)$, where

X_e is a root of $a_0 z^3 + a_1 z^2 + a_2 z + a_3 = 0$, where

$$a_0 = d_{22} > 0,$$
$$a_1 = -d_{23} - d_{22}d_{11} - d_{21}d_{12} - d_{24} + d_{22},$$
$$a_2 = -d_{22}d_{11} - d_{24} + d_{23}d_{11} + d_{24}d_{11},$$
$$a_3 = d_{24}d_{11} > 0.$$

M_e is obtained from $M_e = \frac{-d_{11} - d_{11}X_e + X_e + X_e^2}{d_{12}X_e}$.

The Jacobian of the system (4.1)–(4.2) is:

$$\mathscr{J} = \begin{bmatrix} -\frac{d_{12}M}{(1+X)^2} - 1 & -\frac{d_{12}X}{1+X} \\ d_{21} + d_{22}M - \frac{d_{23}M}{(1+X)^2} & d_{22}X - \frac{d_{23}X}{1+X} - d_{24} \end{bmatrix} = \begin{bmatrix} \Gamma_{11} & \Gamma_{12} \\ \Gamma_{21} & \Gamma_{22} \end{bmatrix}. \tag{4.3}$$

Theorem 1 *The system (4.1)–(4.2) is locally asymptotically stable at $E(X_e, M_e)$ if:*

(i) $d_{22}X_e < \frac{d_{23}X_e}{1+X_e} + d_{24}$ and
(ii) $d_{21} + d_{22}M_e > \frac{d_{23}M_e}{(1+X_e)^2}$.

Proof The Jacobian of the system (4.1)–(4.2) at $E(X_e, M_e)$ is:

$$\mathscr{J}_e = \begin{bmatrix} -\frac{d_{12}M_e}{(1+X_e)^2} - 1 & -\frac{d_{12}X_e}{1+X_e} \\ d_{21} + d_{22}M_e - \frac{d_{23}M_e}{(1+X_e)^2} & d_{22}X_e - \frac{d_{23}X_e}{1+X_e} - d_{24} \end{bmatrix} = \begin{bmatrix} \Gamma_{11e} & \Gamma_{12e} \\ \Gamma_{21e} & \Gamma_{22e} \end{bmatrix}. \tag{4.4}$$

The characteristic equation of $\mathscr{J}_e$ is given by:

$$\mu^2 + A_1\mu + A_2 = 0,$$

where $A_1 = -(\Gamma_{11e} + \Gamma_{22e})$ and $A_2 = (\Gamma_{11e}\Gamma_{22e} - \Gamma_{12e}\Gamma_{21e})$. The system (4.1)–(4.2) is locally asymptotically stable at $E(X_e, M_e)$ if both the eigen-values of $\mathscr{J}_e$ are real negative or complex with negative real parts, i.e., according to Routh–Hurwitz criterion iff $A_1 > 0$ and $A_2 > 0$. Clearly, $\Gamma_{11e} < 0$.

Therefore, if $\Gamma_{22e} < 0$, i.e., $d_{22}X_e < \frac{d_{23}X_e}{1+X_e} + d_{24}$ then $A_1 > 0$. When $\Gamma_{22e} < 0$ holds, and if $\Gamma_{21e} > 0$, then one has $A_2 > 0$. Therefore, the conditions for locally asymptotic stability are (i) $d_{22}X_e < \frac{d_{23}X_e}{1+X_e} + d_{24}$ and (ii) $d_{21} + d_{22}M_e > \frac{d_{23}M_e}{(1+X_e)^2}$. □

Theorem 2 *The system (4.1)–(4.2) is globally stable at $E(X_e, M_e)$ if:*

$$V_{12} + V_{22} < V_{11} + V_{21},$$

where $V_{ij}, i, j = 1, 2$ are defined in the proof.

Proof Consider

$$V = \left(X - X_e - X_e \ln\frac{X}{X_e}\right) + \left(M - M_e - M_e \ln\frac{M}{M_e}\right) = \sum_{i=1}^{2} V_i, \tag{4.5}$$

where $V_i = (f_i - f_{i_e} - f_{i_e} \ln\frac{f_i}{f_{ie}})$, where $f_i = X, M$ for $i = 1, 2$, respectively.

Now, at $E(X_e, M_e)$, the right-hand sides of equations (4.1)–(4.2) are 0, and hence one obtains:

$$d_{11} - d_{12}\frac{M_e X_e}{1+X_e} - X_e = 0$$
$$\implies d_{11} = d_{12}\frac{M_e X_e}{1+X_e} + X_e$$
$$d_{21}X_e + d_{22}X_e M_e - d_{23}\frac{X_e M_e}{1+X_e} - d_{24}M_e = 0$$
$$\implies d_{21} = \frac{1}{X_e}[-d_{22}X_e M_e + d_{23}\frac{X_e M_e}{1+X_e} + d_{24}M_e].$$

Then, using these above equations and performing a straight forward calculation, one may get:

$$\dot{V} = \sum_{i=1}^{2} \dot{V}_i = \sum_{i=1}^{2} \left(1 - \frac{f_{i_e}}{f_i}\right)\dot{f}_i, \tag{4.6}$$

where

$$\dot{V}_1 \leq \underbrace{-(X - X_e)^2}_{-V_{11}} + \underbrace{d_{12}(XX_eM_e + XMX_e)}_{V_{12}}$$

$$\dot{V}_2 \leq \underbrace{-d_{24}X(M - M_e)^2}_{-V_{21}} + \underbrace{d_{24}M(MX + M_eX_e) + d_{22}(XM^2 + XM_e^2) + d_{23}(MX_eM_e + XMM_e)}_{V_{22}}.$$

Hence, if

$$V_{12} + V_{22} < V_{11} + V_{21}, \tag{4.7}$$

then one may have:

$$\dot{V} \leq 0. \tag{4.8}$$

Also from Eq. (4.6), it is clear that $\dot{V} = 0$ at $E(X_e, M_e)$. Hence, by Lyapunov–Lasalle's invariance principle (Hale 1969), the proof follows. □

Bifurcation analysis

Theorem 3 *The system (4.1)–(4.2) exhibits a saddle-node bifurcation around the equilibrium point $E(X_e, M_e)$ at $d_{23} = d_{23}^{[sn]}$.*

Proof Let the Jacobian matrix corresponding to (4.1)–(4.2) at $E(X_e, M_e)$ be:

$$\mathscr{J}_e = \begin{bmatrix} \Gamma_{11e} & \Gamma_{12e} \\ \Gamma_{21e} & \Gamma_{22e} \end{bmatrix}, \tag{4.9}$$

where details of Γ_{ij_e} are provided in (4.4). The matrix $\mathscr{J}$ has a zero eigen-value iff $\det \mathscr{J} = 0$. Solving $\det \mathscr{J} = 0$, one gets: $d_{23} = \frac{-\mathscr{P}}{(1+X_e)X_e} = d_{23}^{[sn]}$, where

$$\begin{aligned} \mathscr{P} = &- d_{22}{X_e}^3 - 2\,d_{22}{X_e}^2 + d_{24}{X_e}^2 + d_{12}{X_e}^2 d_{21} \\ &+ d_{12}M_e d_{22}{X_e}^2 \\ &- d_{22}X_e + d_{12}X_e d_{21} + 2\,d_{24}X_e + d_{12}M_e d_{24} + d_{24}. \end{aligned}$$

The other eigen-values of $\mathscr{J}$ are evaluated at $d_{23} = d_{23}^{[sn]}$, and one of them must be negative to get a saddle-node bifurcation. Let ψ and $\tilde{\psi}$ be the eigen-vectors corresponding to the eigen-value 0 of the matrix $\mathscr{J}$ and its transpose $\mathscr{J}^T$, respectively.

The eigen-vectors are obtained as: $\psi = \begin{bmatrix} \theta_1 \\ \theta_2 \end{bmatrix}$ and $\tilde{\psi} = \begin{bmatrix} \delta_1 \\ \delta_2 \end{bmatrix}$, where θ_k for $k = 1, 2$ are the roots of the system $\sum_{k=1}^{2} \Gamma_{ike}\theta_k = 0$ for $i = 1, 2$ and δ_K for $k = 1, 2$ are the roots of the system $\sum_{k=1}^{4} \Gamma_{kie}\delta_k = 0$ for $i = 1, 2$.

Denote RHS of (4.1)–(4.2) by G. Then, one may evaluate $G_{d_{23}}$. It is clear from the expressions on RHS of (4.1)–(4.2) that $G_{d_{23}} = \begin{bmatrix} 0 \\ \frac{-MX}{1+X} \end{bmatrix}$. Therefore, $G_{d_{23}}(E(X_e, M_e), d_{23}^{[sn]}) = \begin{bmatrix} 0 \\ \frac{-M_e X_e}{1+X_e} \end{bmatrix}$. Therefore, one may obtain then: $\tilde{\psi}^T G_{d_{23}}(E(X_e, M_e), d_{23}^{[sn]}) = -\delta_2 \frac{-M_e X_e}{1+X_e} \neq 0$. Also, one may see that $\tilde{\psi}^T (D^2 G_{d_{23}}(E(X_e, M_e), d_{23}^{[sn]})(\psi, \psi)) \neq 0$, where D^2 operator is explained in detail in Perko (2008). Following **Sotomayor's theorem** given in Perko (2008), one may conclude that at $d_{23} = d_{23}^{[sn]}$, the system (4.1)–(4.2) goes through a saddle-node bifurcation. □

Stability analysis in the presence of diffusion

The spatial model (3.1)–(3.2) is considered in this section. In (3.1)–(3.2), D_1 and D_2 are the dimensionless self-diffusion coefficients of oxidised LDL and macrophages respectively. To study the effect of diffusion in the spatial model (3.1)–(3.2), first, one should linearize the system (3.1)–(3.2) about the non-zero equilibrium $E(X_e, M_e)$ as follows:

$$\frac{\partial U}{\partial t} = \Gamma_{11e}U + \Gamma_{12e}V + D_1\nabla^2 U, \tag{5.1}$$

$$\frac{\partial V}{\partial t} = \Gamma_{21e}U + \Gamma_{22e}V + D_2\nabla^2 V, \tag{5.2}$$

where $X = X_e + U$, $M = M_e + V$, and Γ_{ij_e} has similar expressions as described in Theorem 1 for $i, j = 1, 2$. Here, (U, V) are small perturbations of (X, M) about the equilibrium point $E(X_e, M_e)$. One may assume that

$$\begin{bmatrix} U \\ V \end{bmatrix} = \begin{bmatrix} v_1 \\ v_2 \end{bmatrix} e^{\lambda t + ikx},$$

where $\lambda > 0$, $v_i > 0$ represent the amplitude $(i = 1, 2)$ and k is the wave number of the perturbation in time t. The system (5.1)–(5.2) becomes:

$$\frac{\partial U}{\partial t} = (\Gamma_{11e} - D_1k^2)U + \Gamma_{12e}V, \tag{5.3}$$

$$\frac{\partial V}{\partial t} = \Gamma_{21e}U + (\Gamma_{22e} - D_2k^2)V. \tag{5.4}$$

At $E(X_e, M_e)$, the characteristic equation of the linearised system (5.3)–(5.4) is:

$\lambda^2 + \hat{A}_1\lambda + \hat{A}_2 = 0$,
where $\hat{A}_1 = A_1 + (D_1 + D_2)k^2$ and $\hat{A}_2 = A_2 - (D_1\Gamma_{22e} + D_2\Gamma_{11e})k^2 + D_1D_2k^4$.

Theorem 4 *If $d_{22}X_e < \frac{d_{23}X_e}{1+X_e} + d_{24}$, the stability of the non-spatial system (4.1)–(4.2) at $E(X_e, M_e)$ implies the stability of the diffusive system (3.1)–(3.2).*

Proof The stability of the non-spatial system (4.1)–(4.2) at $E(X_e, M_e)$ implies the stability of the spatial system (3.1)–(3.2) at $E(X_e, M_e)$ if $\hat{A}_1 > 0$ and $\hat{A}_2 > 0$. According to Theorem 1, we have $A_1 > 0$ and $A_2 > 0$. Therefore, clearly,

Table 1 List of parameter values used in the model

Parameters	Description	Numeric values
d_{11}	Cholesterol influx rate	2
d_{12}	Rate of loss of oxidised LDL for consumption by macrophages	0.048
d_{21}	Rate of endothelial response to oxidised LDL	0.1
d_{22}	Rate of endothelial response to macrophages /T-cell cytokines	1
d_{23}	Rate of loss of macrophages for phagocytosing oxidised LDL	0.048
d_{24}	Death rate of macrophages	0.24

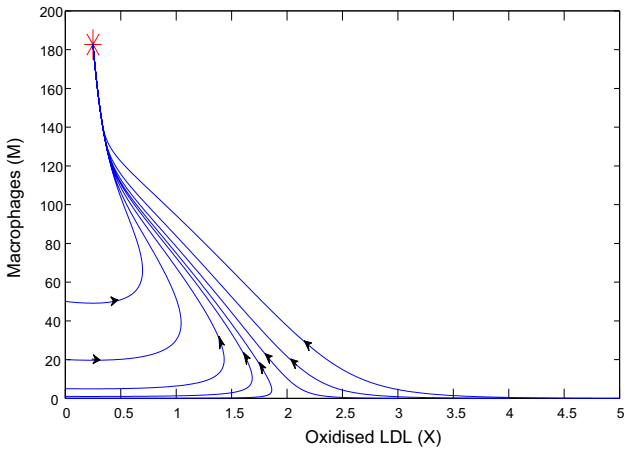

Fig. 2 Local stability of the non-spatial model (4.1)–(4.2) corresponding to the parameter values from Table 1 and the red asterisk denotes the equilibrium point where all the trajectories converge from several initial positions

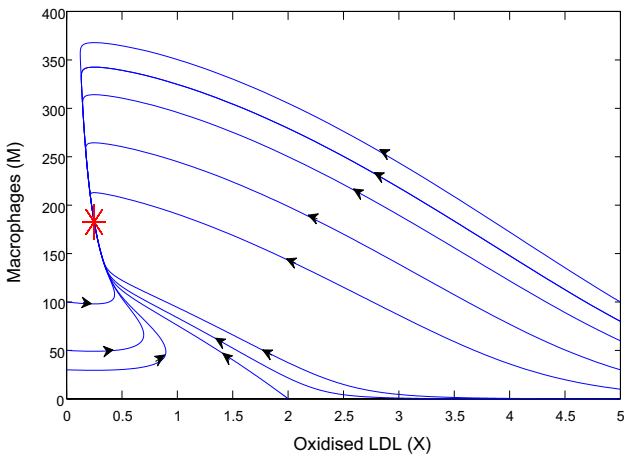

Fig. 3 Global stability of the non-spatial model (4.1)–(4.2) corresponding to the parameter values from Table 1 and the red asterisk denotes the equilibrium point where all the trajectories converge from several initial positions far away from the equilibrium point

$\hat{A_1} > 0$ always. Suppose that $\hat{A}_2 = A_2 - H_1k^2 + H_2k^4$, where $H_1 = D_1\Gamma_{22e} + D_2\Gamma_{11e}$ and $H_2 = D_1D_2$. Clearly $H_2 > 0$. As

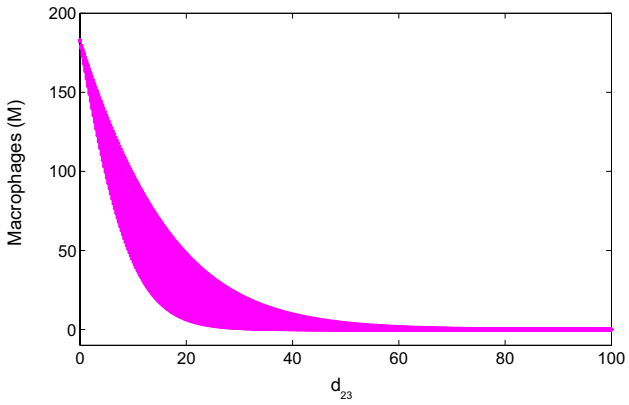

Fig. 4 Bifurcation diagram of macrophages' concentration with respect to d_{23} keeping all other parameter values remain same as of Table 1

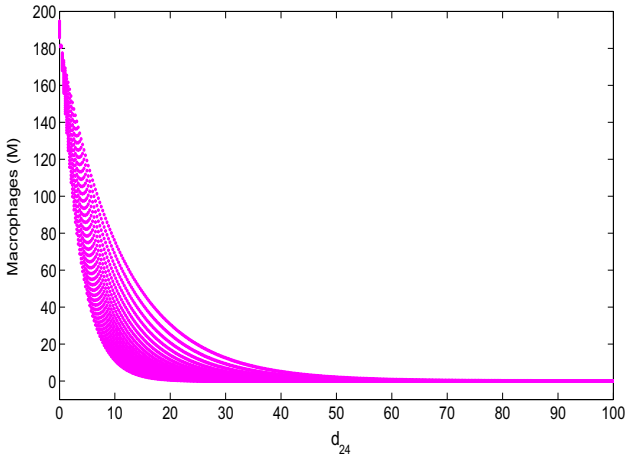

Fig. 5 Bifurcation diagram of macrophages' concentration with respect to d_{24} keeping all other parameter values remain the same as of Table 1

$\Gamma_{11e} < 0$, so $H_1 < 0$ whenever $\Gamma_{22e} < 0$. This proves that the diffusive system is also stable at $E(X_e, M_e)$ under the same condition as of non-spatial system which is expressed as $\Gamma_{22e} < 0$, i.e., $d_{22}X_e < \frac{d_{23}X_e}{1+X_e} + d_{24}$. □

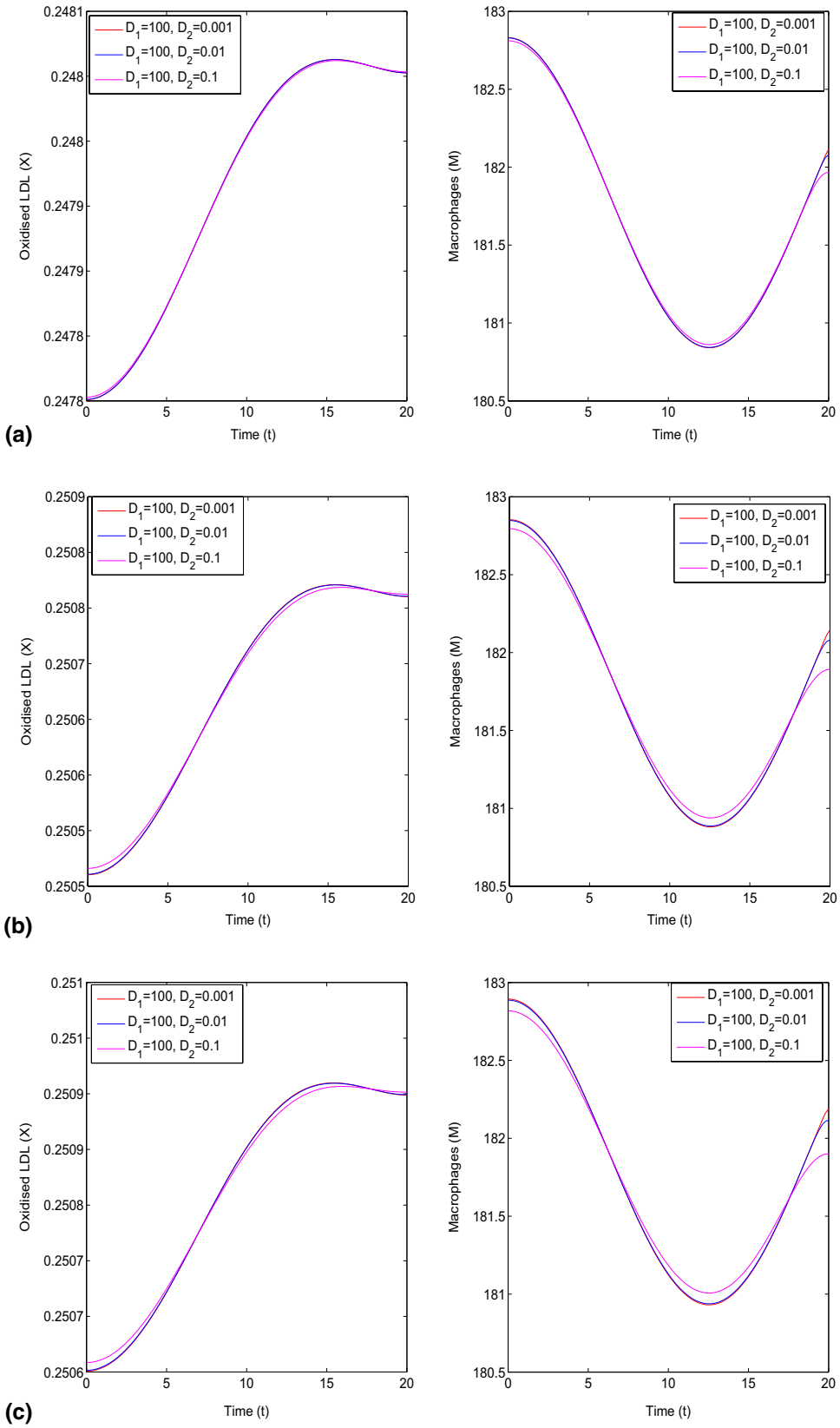

Fig. 6 Panel of time-variant concentrations of oxidised LDL and macrophages corresponding to three different values of D_2 for a fixed D_1 at various specific locations **a** $x = 2$, **b** $x = 4$, **c** $x = 5$

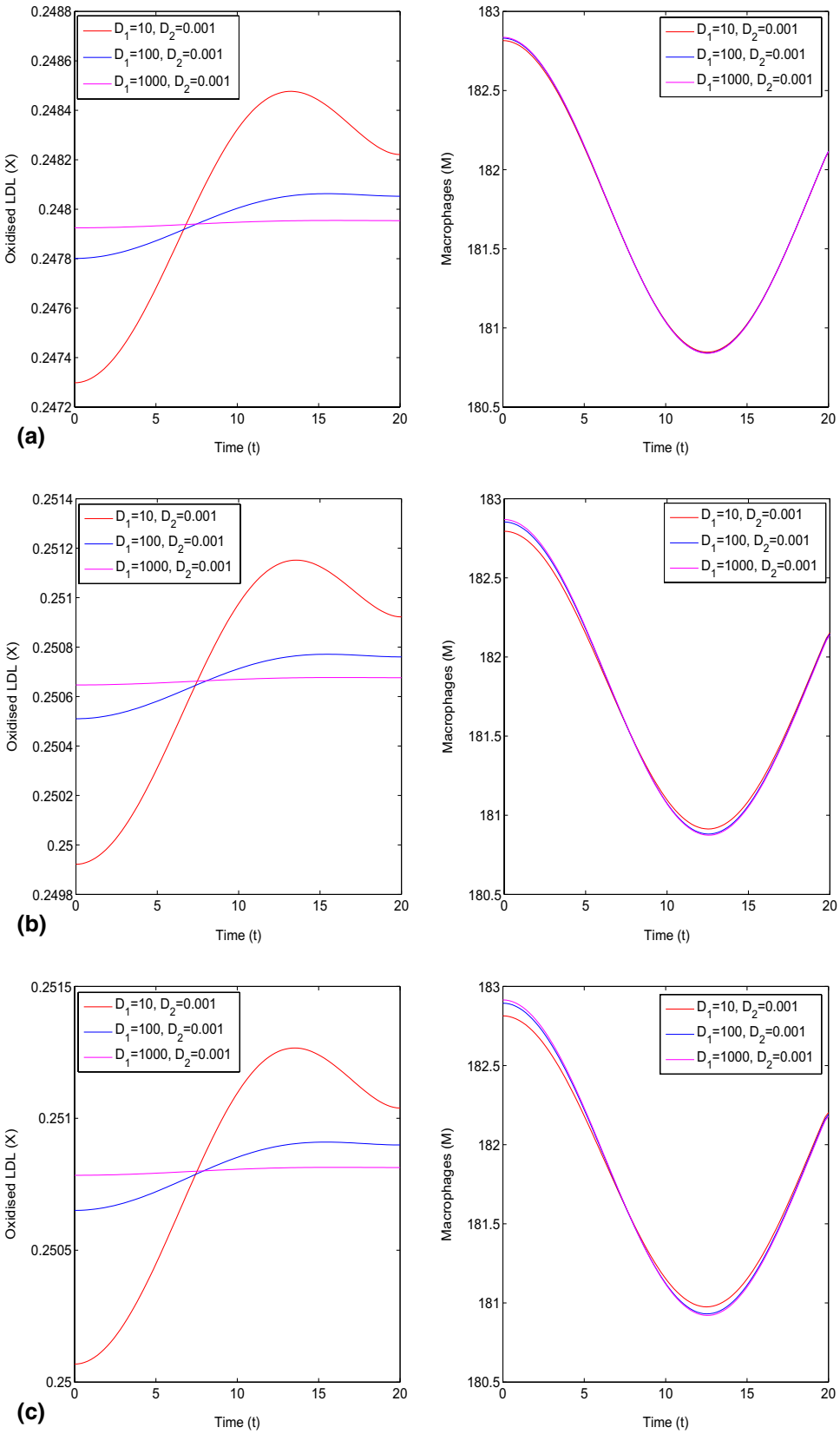

Fig. 7 Panel of time-variant concentrations of oxidised LDL and macrophages corresponding to three different values of D_1 for a fixed D_2 at various specific locations **a** $x = 2$, **b** $x = 4$, **c** $x = 5$

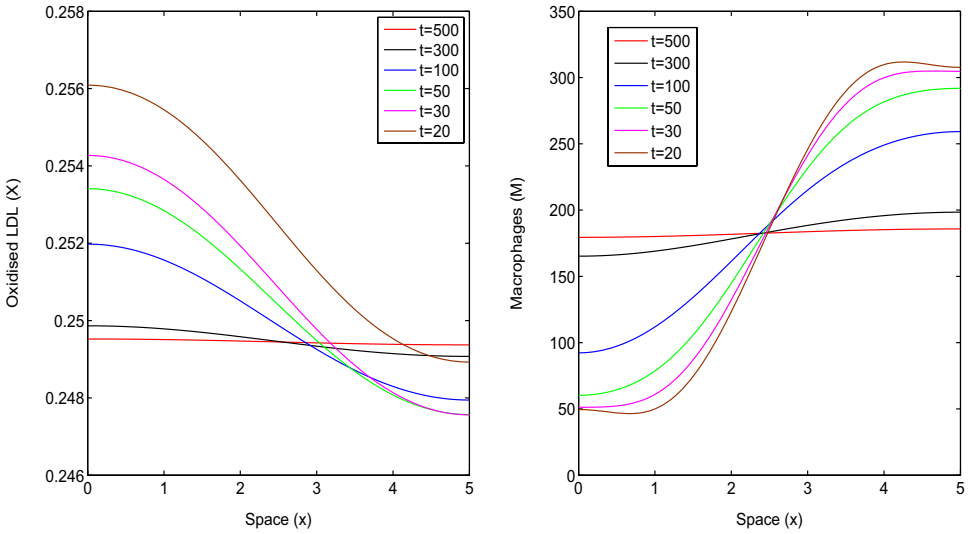

Fig. 8 Spatial pattern of the concentrations of oxidised LDL (in left) and macrophages (in right) for different time periods

Theorem 5 *The condition for diffusive-driven instability of the system at* $E(X_e, M_e)$ *is given by,* $A_2 + H_2k^4 < H_1k^2$, *i.e., if* $A_2 + k^4D_1D_2 < (D_1\Gamma_{22e} + D_2\Gamma_{11e})k^2$.

Proof The spatial system undergoes instability if $\hat{A_2} < 0$. Now, from above $\hat{A}_2 = A_2 - H_1k^2 + H_2k^4$, where $H_1 = D_1\Gamma_{22e} + D_2\Gamma_{11e}$ and $H_2 = D_1D_2$. Therefore, $\hat{A_2} < 0$ if $A_2 + H_2k^4 < H_1k^2$, i.e., if $A_2 + k^4D_1D_2 < (D_1\Gamma_{22e} + D_2\Gamma_{11e})k^2$.

Numerical simulation

This section provides various numerical simulations for both the non-spatial (4.1)–(4.2) and spatial (3.1)–(3.2) dynamical system under consideration with the model parameters included in Table 1. The non-negative equilibrium point $E(X_e, M_e)$ of the non-spatial model (4.1)–(4.2) is found to be $X_e = 0.2494464334$, $M_e = 182.6730627$, and the eigen-values of $\mathscr{J}_e$ at this equilibrium point are found to be $-6.349, -0.268$, thereby ensuring the stability nature of the model system under the usage of the parameter values provided in Table 1. Figure 2 depicts the locally asymptotically stable nature of the non-spatial model system around the equilibrium point, whereas Fig. 3 shows the global stability irrespective of the starting positions. Thus, the stability of equilibrium position for non-spatial model system is established both analytically and numerically.

Figure 4 displays a bifurcation diagram of macrophages with respect to the model parameter d_{23} of the non-spatial model (4.1)–(4.2) over the specific range $0 \le d_{23} \le 60$ while keeping all the remaining parameter values unaltered as enlisted in Table 1. The instability occurs in the region which is $0 \le d_{23} \le 60$. The biological interpretation of the bifurcation diagram may be made in a way that in the event of decreasing the rate of loss of macrophages for phagocytosing oxidised LDL, the foam cell formation gradually reaches a threshold level resulting in rupturing of endothelium wall and plaque bulges into lumen obstructing the smooth blood flow, and hence, an instability occurs in the vascular region (Davis 2005).

On the other hand, the dynamical behaviour of concentration of macrophages also experiences a bifurcation with respect to d_{24}, as depicted in Fig. 5. The bifurcation diagram is plotted by treating concentration of macrophage as a function of d_{24} with the range of values $0 \le d_{24} \le 100$. The chaotic region is observed for the range $0 \le d_{24} \le 50$ and beyond which the stability has been found to prevail because of period halving experience of the model system. From biological point of view, this diagram ensures that when the death rate of macrophage decreases, the number of active macrophage increases in the intima to consume more oxidised LDL, and hence, accumulation of plaque increases eventually leading to the instability of the vascular region (Libby et al. 2002).

The panel of pictures exhibited in Fig. 6 illustrates the characteristic of time-variant concentrations of oxidised LDL and macrophages corresponding to three different values of $D_2 = 0.001, 0.01$ and 0.1 for a specific value of $D_1 = 10^2$ at three spatial locations of $x = 2, 4$ and $x = 5$. It appears that the decreasing diffusivity of the macrophages causes an enhancement of the oxidised LDL and reduction of macrophages at the onset resulting in a gradual increasing–decreasing trend for oxidised LDL and reverse decreasing–increasing trend for macrophages with large passage of time. These trends are maintained at all the spatial sites differing only in the vicinity of equilibrium position. One may note from these pictures that the deviations prevailed more

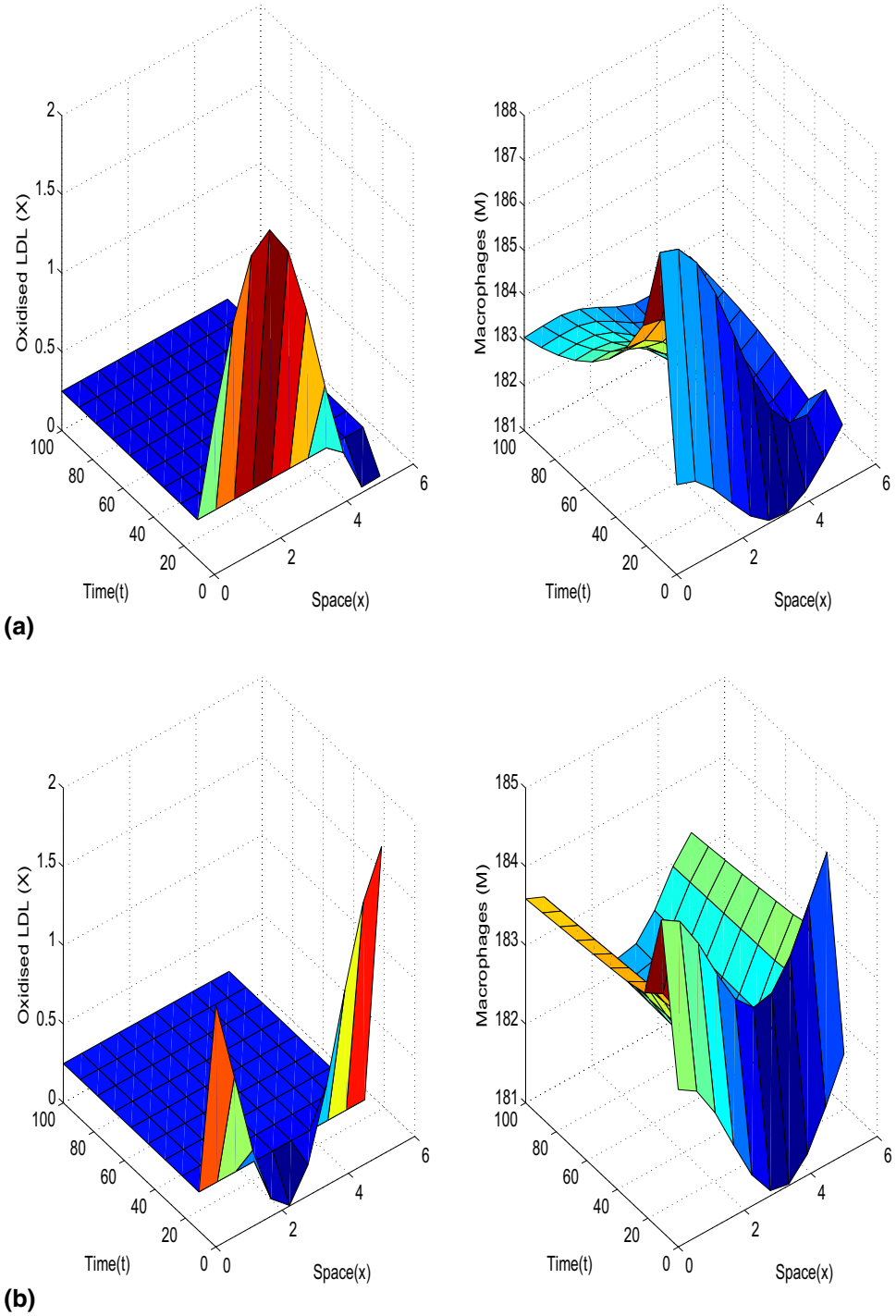

Fig. 9 **a** Distribution of oxidised LDL (X) and macrophages (M) over time and space of the present model (3.1)–(3.2) for diffusion coefficients $D_1 = 100$ and $D_2 = 0.001$, while other parameter values remain the same with initial condition (IC) $=[1 + \cos(x), 182 + \cos(x)]$. **b** Distribution of oxidised LDL (X) and macrophages (M) over time and space of the model (3.1)–(3.2) for diffusion coefficients $D_1 = 10^3$ and $D_2 = 0.001$ keeping other parameter values same with IC$=[1 + \cos(x), 182 + \cos(x)]$

towards the onset and they gradually die out towards the end after considerable advancement of time.

On the other hand, the nature of the variations of concentrations of oxidised LDL and macrophages with time at different spatial locations are captured in Fig. 7 corresponding to three values of $D_1 = 10, 10^2$, and 10^3 for a specific value of $D_2 = 0.001$. The enhanced diffusivity of oxidised LDL concentration causes it to increase with time right from its onset followed by a slight diminishing trend towards the advancement of time. A completely reverse trend is observed in the concentration of macrophages. The deviations of magnitudes for both the concentrations of oxidised LDL and macrophages over the entire span of time at all the selected spatial locations are recorded to vary within the vicinity of

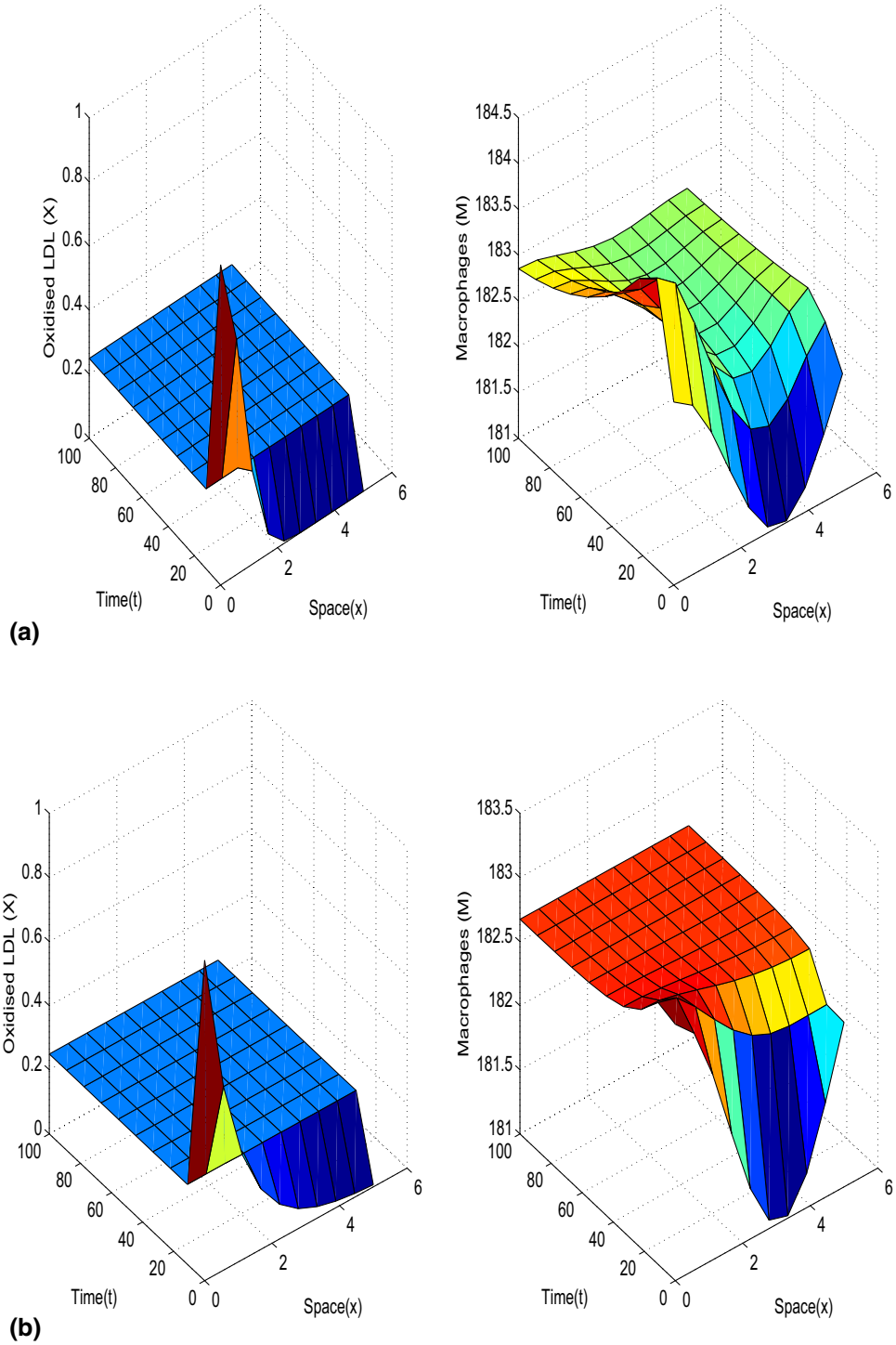

Fig. 10 **a** Distribution of oxidised LDL (X) and macrophages (M) over time and space of the present model (3.1)–(3.2) for diffusion coefficients $D_1 = 10^2$ and $D_2 = 0.01$ and other parameter values remain the same with IC=$[1 + \cos(x), 182 + \cos(x)]$. **b** Distribution of oxidised LDL (X) and macrophages (M) over time and space of the model (3.1)–(3.2) for diffusion coefficients $D_1 = 10^2$ and $D_2 = 0.001$ keeping other parameter values same with IC=$[1 + \cos(x), 182 + \cos(x)]$

the equilibrium position of the present system. Such deviations appear to be more towards the outer boundary $x = 5$ than near the inner one $x = 2$.

Figure 8 includes the spatial patterns of the concentrations of oxidised LDL and macrophages over the entire space length for different time periods. One may note that the oxidised LDL keeps on diminishing spatially from one end to the other for all time periods, but the diminishing rate is gradually decreasing with increasing time in such a way that the profile becomes almost constant for $t = 500$ having zero slope. The macrophage concentration, on the other hand, follows a reverse spatial pattern of increasing trend from one end to the other, the rate of which gradually decreases with increasing time, and at one stage $t = 500$, it comes almost a straight line as in the case of oxidised LDL. Therefore, examining the behaviour of spatial patterns, one

may note that both the patterns gradually reduce to almost straight lines assuming their respective concentrations in the vicinity of the equilibrium position irrespective of the spatial locations. In other words, the present spatial model system bears the potential to establish its stability right from the characteristics of the spatial patterns, especially how they approach the equilibrium state with large passage of time.

The distributions of oxidised LDL and macrophages in the system under consideration in the three-dimensional space are recorded in Fig. 9 for two different values of diffusivity ($D_1 = 100, 1000$) of the oxidised LDL while keeping a constant diffusivity of the macrophages. It appears from the pictures (a) and (b) that in the event of increasing diffusivity of the oxidised LDL from 100 to 1000, the shape of the distribution of both oxidised LDL and macrophages gets largely perturbed with an increasing and decreasing trend, respectively, with time advancement, while a reverse trend is followed spatially. In an analogous manner, one may observe the change of the shape of the distribution corresponding to the different diffusivity of macrophages ($D_2 = 0.01, 0.001$) for a constant diffusivity ($D_1 = 10^2$) of oxidised LDL, exhibited in the concluding Fig. 10. Studying the characteristics of all the shapes in three-dimensional space, one may estimate the effects of diffusivity (D_1, D_2) on the distribution of oxidised LDL and macrophages over space and time in the system under consideration.

Concluding remarks

The present article deals with a reaction–diffusion system in one-dimensional space to describe the basic interaction of oxidised LDL and macrophages in the intima for atherosclerotic plaque formation. The corresponding non-spatial model has been found to be locally and globally stable around the positive equilibrium. One of the important features of this model is the global stability of the non-spatial model. The existence of global stability which is very rare in previous studies comprising mathematical models for the study of atherosclerosis implies that it can withstand to some extent a significant change in the numerical values of parameters involved in the model. The dynamical system experiences bifurcation with respect to some significant parameters having relevant biological interpretations. In addition, the diffusive system is found to be stable under suitable conditions involving the model parameters and self-diffusion coefficients. The stability of the system under consideration irrespective of spatial and non-spatial character is established both analytically and numerically. The spatial patterns are found to have a tendency to approach the stable equilibrium position with the advancement of time. Moreover, diffusivity of the oxidised LDL concentration has got its importance more than that of macrophages on the distribution of these cellular components over space and time.

Acknowledgements The authors gratefully acknowledge the financial support by Special Assistance Programme (SAP-III) sponsored by the University Grants Commission (UGC), New Delhi, India [Grant nos. F.510/3/DRS-III/2015(SAP-I)].

References

Anlamlert W, Lenbury Y, Bell J (2017) Modeling fibrous cap formation in atherosclerotic plaque development: stability and oscillatory behavior. Adv Diff Equ

Bulelzai MA, Dubbeldam JL (2012) Long time evolution of atherosclerotic plaques. J Theor Biol 297:1

Cobbold C, Sherratt J, Maxwell S (2002) Lipoprotein oxidation and its significance for atherosclerosis: a mathematical approach. Bull Math Biol 64(1):65

Cohen A, Myerscough MR, Thompson RS (2014) Athero-protective effects of high density lipoproteins (HDL): an ODE model of the early stages of atherosclerosis. Bull Math Biol 76(5):1117

Davis NE (2005) Atherosclerosis-an inflammatory process. J Insur Med 37(1):72

Friedman A, Hao W (2015) A mathematical model of atherosclerosis with reverse cholesterol transport and associated risk factors. Bull Math Biol 77(5):758

Gijsen FJ, Wentzel JJ, Thury A, Mastik F, Schaar JA, Schuurbiers JC, Slager CJ, van der Giessen WJ, de Feyter PJ, Van der Steen AF, Serruys PW (2008) Strain distribution over plaques in human coronary arteries relates to shear stress. Am J Physiol Heart Circ Physiol 295(4):H1608

Gui T, Shimokado A, Sun Y, Akasaka T, Muragaki Y (2012) Diverse roles of macrophages in atherosclerosis: from inflammatory biology to biomarker discovery. Mediat Inflamm

Guo M, Cai Y, Yao X, Li Z (2018) Mathematical modeling of atherosclerotic plaque destabilization: role of neovascularization and intraplaque hemorrhage. J Theor Biol 450:53

Hale JK (1969) Ordinary differential equations. Pure and Applied Mathematics. Wiley-Interscience, Hoboken

Hao W, Friedman A (2014) The LDL–HDL profile determines the risk of atherosclerosis: a mathematical model. PLoS One 9(3):e90497

Ibragimov A, McNeal C, Ritter L, Walton J (2005) A mathematical model of atherogenesis as an inflammatory response. Math Med Biol 22(4):305

Johnson JL, Newby AC (2009) Macrophage heterogeneity in atherosclerotic plaques. Curr Opin Lipidol 20(5)

Libby P, Ridker PM, Maseri A (2002) Inflammation and atherosclerosis. Circulation 105(9):1135

Little MP, Gola A, Tzoulaki I (2009) A model of cardiovascular disease giving a plausible mechanism for the effect of fractionated low-dose ionizing radiation exposure. PLoS Comput Biol 5(10):e1000539

Malek AM, Alper SL, Izumo S (1999) Hemodynamic shear stress and its role in atherosclerosis. JAMA 282(21):2035

McKay C, McKee S, Mottram N, Mulholland T, Wilson S, Kennedy S, Wadsworth R (2005) Towards a model of atherosclerosis. University of Strathclyde

Mukherjee D, Guin LN, Chakravarty S (2019) Dynamical response of atherosclerotic plaque through mathematical model. Biophys Rev Lett. https://doi.org/10.1142/S1793048019500036

Ougrinovskaia A, Thompson RS, Myerscough MR (2010) An ODE model of early stages of atherosclerosis: mechanisms of the inflammatory response. Bull Math Biol 72(6):1534

Parton A, McGilligan V, O'kane M, Baldrick FR, Watterson S (2015) Computational modelling of atherosclerosis. Brief Bioinf 17(4):562

Perko L (2008) Differential equations and dynamical systems. Texts in applied mathematics. Springer, New York

Pittilo M (2000) Cigarette smoking, endothelial injury and cardiovascular disease. Int J Exp Pathol 81(4):219

Watson MG, Byrne HM, Macaskill C, Myerscough MR (2018) A two-phase model of early fibrous cap formation in atherosclerosis. J Theor Biol 456:123